

SYSTOLES OF HYPERBOLIC SURFACES WITH BIG CYCLIC SYMMETRY

SHENG BAI, YUE GAO, AND SHICHENG WANG

ABSTRACT. We obtain the exact values of the systoles of these hyperbolic surfaces of genus g with cyclic symmetries of the maximum order and the next maximum order. Precisely: for genus g hyperbolic surface with order $4g + 2$ cyclic symmetry, the systole is $2 \operatorname{arccosh}(1 + \cos \frac{\pi}{2g+1} + \cos \frac{2\pi}{2g+1})$ when $g \geq 7$, and for genus g hyperbolic surface with order $4g$ cyclic symmetry, the systole is $2 \operatorname{arccosh}(1 + 2 \cos \frac{\pi}{2g})$ when $g \geq 4$.

CONTENTS

1. Introduction	1
2. Uniqueness of hyperbolic Σ_g which admits big cyclic symmetry	3
3. Trigonometric formulae	4
4. Polygon modules of hyperbolic surfaces and candidates of systoles	7
4.1. Polygon modules	8
4.2. Candidates of systoles	9
5. Injective radius h_i	11
5.1. Some reductions	11
5.2. Lift $B(x, h_i)$ to the universal cover	12
5.3. Back to P	17
6. Appendix	23
References	24

1. INTRODUCTION

In this note all surfaces are closed and orientable, all symmetries on surfaces are orientation preserving. When we talk about symmetries on hyperbolic surfaces, we assume those symmetries are isometries.

Hyperbolic surface is a fundamental research object in mathematics with a quite long history. Systole is an important topic in this research. Systole on a closed hyperbolic surface indicates either a shortest closed geodesic or its length, and we often used for latter. For a survey on the study of the systole, see Parlier [Par14].

Below we just list some results which close to our result. F. Jenni [Jen84] got the maximal systole of genus 2 surfaces and C. Bavard [Bav92] got that of genus 2 and 5 hyperelliptic surfaces. P. Schmutz [Sch93] obtained the systole of some surfaces constructed from convex uniform polyhedra with genus 3, 4, 5, 11, 23, 59.

In a rather different way, P. Buser and P. C. Sarnak ([BS94] constructed closed hyperbolic surfaces whose systole has a near-optimal asymptotic behavior with

Genus	$\text{sys}(\Sigma_g^1)$	Genus	$\text{sys}(\Sigma_g^2)$
4	3.41464123	7	3.44730852
5	3.45497357	8	3.46473555
6	3.47667914	9	3.47691634
7	3.48969921	10	3.48576585

TABLE 1.

respect to the genus of the surface by arithmetic methods. Later Katz, Schaps and Vishne [KSV07] found a family of surface with Hurwitz symmetry and with systole not smaller than $4/3 \log g$. See [PW15] and [Pet18] for more recent examples.

Our work is partly inspired by the work [KSV07]: Classical results claims that if a finite group G acts on Σ_g , then $|G| \leq 84(g-1)$ (A. Hurwitz, [Hu]), and moreover $|G| \leq 4g+2$ if G is cyclic (A. Wiman [Wim95]). Call a topological/hyperbolic surface Σ_g has Hurwitz symmetry, if it admits a finite group action of order $84(g-1)$ and has Wiman symmetry if it admits a cyclic finite group action of order $4g+2$. Note it is known for infinitely many g , topological surface Σ_g has Hurwitz symmetry, and for every $g > 1$, topological surface Σ_g has Wiman symmetry. Moreover it is also well known that the next biggest cyclic symmetry on topological surface Σ_g has order $4g$ [Kul97]. It is a classical result that each periodical map f on Σ_g can be realized as an isometry for some hyperbolic structure ρ on Σ_g .

Our result is

Theorem 1. *Suppose Σ_g^1 and Σ_g^2 are hyperbolic surfaces with cyclic symmetry of order $4g$ and $4g+2$ respectively. Then*

$$\text{sys}(\Sigma_g^1) = 2 \operatorname{arccosh}(1 + 2 \cos \frac{\pi}{2g}) \quad \text{for } g \geq 4$$

$$\text{sys}(\Sigma_g^2) = 2 \operatorname{arccosh}(1 + \cos \frac{\pi}{2g+1} + \cos \frac{2\pi}{2g+1}) \quad \text{for } g \geq 7$$

We list some values of the systoles, see Table 1.

From the proof of the theorem, we have

Corollary 1. *In Σ_g^1 , there are $2g$ closed geodesics having length $\text{sys}(\Sigma_g^1)$ and in Σ_g^2 , there are $2g+1$ closed geodesics having length $\text{sys}(\Sigma_g^2)$.*

The method to prove above result is rather direct, and seems different from previous work we mentioned.

We first verify the hyperbolic structure of Σ_g with isometries of big order is unique up to homeomorphism of Σ_g . Then we just pick a well known model of hyperbolic surface Σ_g with isometries of order $4g$ (respectively $4g+2$). In this Σ_g , we conjecture a simple closed geodesic γ realizing the systole. We calculate the length $2h$ of γ . Then we devote to the proof that the injective radius of Σ_g is h .

In Section 2 we verify the uniqueness of hyperbolic structure of Σ_g with isometries of big order. In section 3, we give some trigonometric formulae which will be used later. Some formulae are copied from [Bus10] and some are derived by us. Theorem 1 is proved in Section 4 and Section 5.

The paper is self-contained up to several standard text book.

Acknowledgement: We thank Professor Ursula Hamenstädt for helpful communication. The authors are supported by grant No.11711021 of the National Natural Science Foundation of China.

2. UNIQUENESS OF HYPERBOLIC Σ_g WHICH ADMITS BIG CYCLIC SYMMETRY

Let $S^2(p, q, r)$ denote the hyperbolic orbifold with base space S^2 and 3 singular points of index p, q, r respectively, where p, q, r are three positive integers.

Proposition 1. *Let G_i be a cyclic group action on hyperbolic surface (Σ_g, ρ_i) , $i = 1, 2$, such that*

(1) *those two actions are conjugated,*

(2) $\Sigma_g/G_i = S^2(p, q, r)$.

Then those two hyperbolic metric ρ_1 and ρ_2 on Σ_g are isometric.

Proof. For short, we write $\Sigma_g^i = (\Sigma_g, \rho_i)$. By (1) we have a homeomorphism $\phi : \Sigma_g^1 \rightarrow \Sigma_g^2$ such that $G_2 = \phi G_1 \phi^{-1}$. By choosing the suitable generators σ_1, σ_2 of G_1 and G_2 , we may have $G_1 = \langle \sigma_1 \rangle$, $G_2 = \langle \sigma_2 \rangle$, and $\sigma_2 = \phi \sigma_1 \phi^{-1}$. σ_1, σ_2 are isometries on Σ_g^1 and Σ_g^2 respectively. There is a commute diagram:

$$(2.1) \quad \begin{array}{ccc} \Sigma_g^1 & \xrightarrow{\phi} & \Sigma_g^2 \\ \downarrow \pi_1 & & \downarrow \pi_2 \\ \Sigma_g^1/\sigma_1 & \xrightarrow{\bar{\phi}} & \Sigma_g^2/\sigma_2 \end{array}$$

π_1 and π_2 are the branch covers induced by σ_1, σ_2 . ϕ and $\bar{\phi}$ are homeomorphisms between Σ_g^1 and Σ_g^2 , Σ_g^1/σ_1 and Σ_g^2/σ_2 respectively. Both Σ_g^1/σ_1 and Σ_g^2/σ_2 are the hyperbolic orbifold $S^2(p, q, r)$.

What we need to prove is that there are isometries $\psi, \bar{\psi}$ between Σ_g^1 and Σ_g^2 , Σ_g^1/σ_1 and Σ_g^2/σ_2 respectively, satisfying the commute diagram (2.2).

The hyperbolic structure of the orbifold $S^2(p, q, r)$ is unique, Since it is obtained by doubling two hyperbolic triangles $\Delta(p, q, r)$ of angles $\pi/p, \pi/q, \pi/r$, and the $\Delta(p, q, r)$ is unique.

For a homeomorphism $\bar{\phi}$ on hyperbolic orbifold $S^2(p, q, r)$ that satisfies the diagram (2.1), we are going to prove that $\bar{\phi}$ is isotopic to an isometry $\bar{\psi}$.

$$(2.2) \quad \begin{array}{ccc} \Sigma_g^1 & \xrightarrow{\psi} & \Sigma_g^2 \\ \downarrow \pi_1 & & \downarrow \pi_2 \\ \Sigma_g^1/\sigma_1 & \xrightarrow{\bar{\psi}} & \Sigma_g^2/\sigma_2 \end{array}$$

For convenience, we just denote the singular points of the orbifold $S^2(p, q, r)$ by p, q, r respectively.

We assume l is the shortest geodesic connecting p and q . Then $\bar{\phi}(l)$ is a curve connecting $\bar{\phi}(p)$ and $\bar{\phi}(q)$. By the definition of homeomorphism between orbifolds, $\bar{\phi}(p)$ and p are singular points on the orbifold with the same order and $\bar{\phi}(q)$ and q are singular points on the orbifold with the same order too. Without loss of generality, we assume that $\bar{\phi}(p) = p$ and $\bar{\phi}(q) = q$.

$|S^2(p, q, r) \setminus \{r\}|$ is an open disk. By the contractability of disks, l is isotopic to $\bar{\phi}(l)$ by an isotopy on $S^2(p, q, r) \setminus \{r\}$. So we may assume that $\bar{\phi}$ is already the identity on l .

Similarly, consider the shortest geodesic m between p and r , $\bar{\phi}(m)$ is isotopic to m in $S^2(p, q, r) \setminus l$.

Futhermore, the shortest geodesic n between q and r , $\bar{\phi}(n)$ is isotopic to n in $S^2(p, q, r) \setminus (l \cup m)$.

Then there is a homeomorphism $\bar{\psi}$ on the orbifold isotopic to $\bar{\phi}$ and $\bar{\psi}|_{l \cup m \cup n} = id$.

Then since $S^2(p, q, r) \setminus (l \cup m \cup n)$ consists of two congruent triangles, clearly the restriction of $\bar{\psi}$ on each triangle is isotopic to the identity, and we get that $\bar{\phi}$ is isotopic to the isometry $\bar{\psi}$.

$\bar{\psi}$ can be lifted to a homeomorphism ψ between Σ_g^1 and Σ_g^2 that satisfies the diagram (2.2) and is isotopic to ϕ . Since $\bar{\psi} \circ \pi_1$ and π_2 are local isometry, ψ is a local isometry. Since ψ is bijective, ψ is an isometry. \square

Corollary 2. *The hyperbolic structure of surface Σ_g with cyclic symmetry of order k is unique for $k = 4g + 2$ and $4g$.*

Proof. If G is a cyclic group action of order $4g$ on the hyperbolic surfaces Σ_g , then the orbifold Σ_g/G is $S^2(4g, 4g, 2)$.

If G is a cyclic group action of order $4g + 2$ on the hyperbolic surfaces Σ_g , then the orbifold Σ_g/G is $S^2(4g + 2, 2g + 1, 2)$.

It is well-known that any two cyclic group action of order k on Σ_g is unique up to conjugacy, see [Kul97], or quick argument in [GWWZ15], where $k = 4g$ or $4g + 2$.

By Proposition 1, the corollary follows. \square

3. TRIGONOMETRIC FORMULAE

Below are the trigonometric formulae we use in this work:

A. $\cosh 2x = 2 \cosh^2 x - 1 = 2 \sinh^2 x + 1$

Since

$$\begin{aligned} (e^x + e^{-x})^2 &= e^{2x} + e^{-2x} + 2 \\ (2 \cosh x)^2 &= 2 \cosh 2x + 2, \end{aligned}$$

therefore

$$(3.1) \quad \cosh 2x = 2 \cosh^2 x - 1 = 2 \sinh^2 x + 1.$$

B. Right angle triangle (Figure 1) [Bus10, p.454]

$$(3.2) \quad \cosh c = \cosh a \cosh b.$$

$$(3.3) \quad \sinh a = \sin \alpha \sinh c.$$

$$(3.4) \quad \cos \alpha = \cosh a \sin \beta.$$

C. Cosine law and sine law of hyperbolic triangles (Figure 2) [Bus10, p.454]

$$(3.5) \quad \cosh c = -\sinh a \sinh b \cos C + \cosh a \cosh b.$$

$$(3.6) \quad \frac{\sinh a}{\sin A} = \frac{\sinh b}{\sin B}.$$

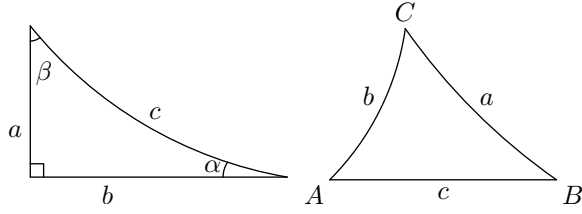


FIGURE 1.

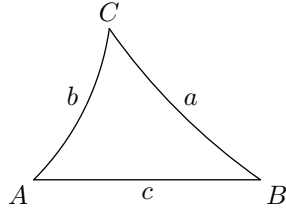


FIGURE 2.

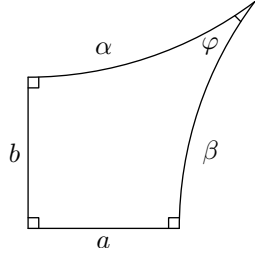


FIGURE 3.

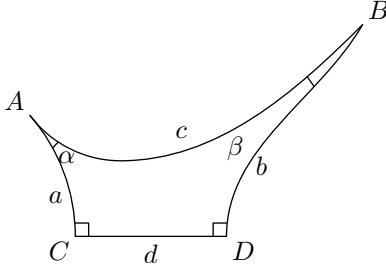


FIGURE 4.

D. Trirectangle (Figure 3) [Bus10, p.454]

$$(3.7) \quad \cosh a = \cosh \alpha \sin \varphi.$$

$$(3.8) \quad \sinh \alpha = \sinh a \cosh \beta.$$

$$(3.9) \quad \sinh \alpha = \coth b \cot \varphi.$$

E. Quadrilateral with two right angles (Figure 4)

$$(3.10) \quad \cosh c = \cosh d \cosh a \cosh b - \sinh a \sinh b.$$

$$(3.11) \quad \cosh d = \sin \alpha \sin \beta \cosh c - \cos \alpha \cos \beta.$$

Below are the proofs for the last two formulae:

Proof of (3.10). In Figure 5, in $\triangle BCD$, we have $\cosh e = \cosh b \cosh d$ by (3.2), and $\sin \angle BCD = \sinh b / \sinh e$ by (3.3).

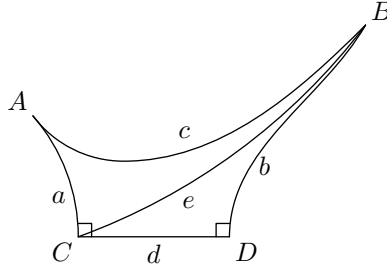


FIGURE 5.

Then in $\triangle ACB$, $\cosh c = -\sinh a \sinh e \cos \angle ACB + \cosh a \cosh e$ by (3.5). Since $\angle BCD + \angle ACB = \pi/2$, we have $\cos \angle ACB = \sin \angle BCD$. By (3.3) we have

$\sin \angle BCD = \frac{\sinh b}{\sinh e}$. Plug the second and third formula into the first formula, we obtain (3.10). \square

Proof of (3.11). We put the quadrilateral in upper half plane. For points in the real line, we will talk their coordinates and additions as real numbers.

The quadrilateral $ACDB$ in Figure 4 is corresponding to the quadrilateral $T_1 R_1 R_2 T_2$ in Figure 6. In this quadrilateral, $\angle T_1 = \alpha$, $\angle T_2 = \beta$, $\angle R_1 = \angle R_2 = \pi/2$. The length of $T_1 T_2 = c$. We hope to obtain the length of $R_1 R_2$, (denoted d).

We assume the coordinate of T_1 to be i , T_2 to be ie^c . In Figure 6, let A, B be the centers of small and big half circles respectively, and r, R be the radius of small and big half circles respectively. By Euclidean trigonometry, in $\triangle AT_1 O$, $\angle O = \pi/2$, $\angle A = \alpha$. In $\triangle BT_2 O$, $OT_2 = e^c$ and $\angle B = \beta$, so we have

$$(3.12) \quad A = \cot \alpha, \quad r = 1/\sin \alpha, \quad B = -e^c \cot \beta, \quad R = e^c/\sin \beta,$$

Respectively the coordinate of C, D, E, F are $A - r, A + r, B - R, B + R$.

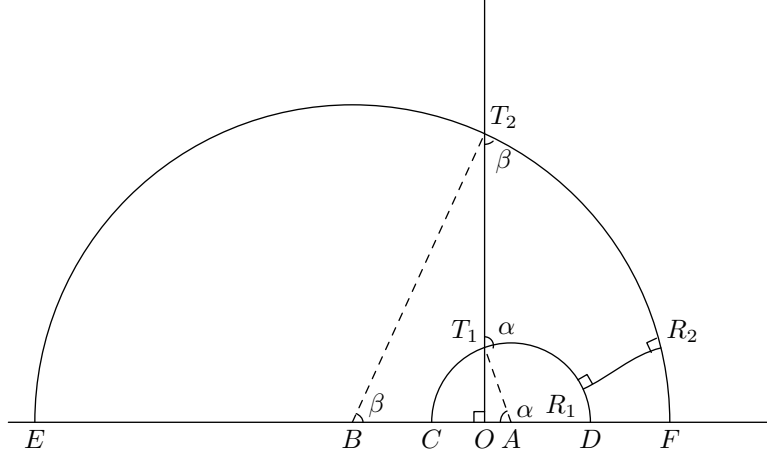


FIGURE 6.

To get $|R_1 R_2|$ we need the isometry φ of \mathbb{H}^2 below which sends $B - R$ to ∞ , where

$$\varphi : z \mapsto -1/(z - (B - R)).$$

Figure 7 is the image of Figure 6 under φ , and E', F', C', D' are the images of E, F, C, D under φ respectively. Their coordinates in Figure 7 are list below by the coordinates of their preimages in Figure 6.

$$(3.13) \quad E' = \infty, \quad F' = -\frac{1}{2R}, \quad C' = \frac{-1}{A - r - (B - R)}, \quad D' = \frac{-1}{A + r - (B - R)}.$$

We denote the center of the halfcircle as P .

We figure out the formula of the length $|R'_1 R'_2|$:

$$(3.14) \quad |R'_1 R'_2| = \operatorname{arccosh} \frac{1}{\cos \angle R'_1 F' R'_2}.$$

In this proof, to avoid confusions, we denote the hyperbolic distance between two points A and B as $|AB|$, the Euclidean distance between them as $|AB|_e$.

Since $\angle R'_2 F' P = \angle P R'_1 F' = \pi/2$, then $\angle R'_1 F' R'_2 = \angle R'_1 P F'$. Thus

$$\cos \angle R'_1 F' R'_2 = \cos \angle R'_1 P F' = \frac{|R'_1 P|_e}{|P F'|_e}.$$

The Euclidean distance $|R'_1 P|_e$, $|P F'|_e$ is obtained directly by the coordinates of the points. Here $|P R'_1|_e = |P D'|_e = |C' D'|_e/2$. Therefore

$$\begin{aligned} \cosh |R_1 R_2| &= \frac{1}{\cos \angle R'_1 F' R'_2} = \frac{1}{\cos \angle R'_1 P F'} = \frac{|F' P|_e}{|P R'_1|_e} \\ &= \frac{-\frac{1}{2R} + (\frac{1}{A-r-(B-R)} + \frac{1}{A+r-(B-R)})/2}{(\frac{1}{A-r-(B-R)} - \frac{1}{A+r-(B-R)})/2} \quad (\text{by plugging (3.13)}) \\ &= \frac{2(A-B+R) - \frac{(A-B+R)^2 - r^2}{R}}{2r} \\ &= \frac{2(A-B+R)R - (A-B+R)^2 + r^2}{2Rr} \\ &= \frac{R^2 - (A-B)^2 + r^2}{2Rr} \\ &= \frac{e^{2c} \sin^2 \alpha - (\cos \alpha \sin \beta + e^c \sin \alpha \cos \beta)^2 + \sin^2 \beta}{2e^c \sin \alpha \sin \beta} \quad (\text{by plugging (3.12)}) \\ &= \frac{e^{2c} \sin^2 \alpha + \sin^2 \beta - (\cos^2 \alpha \sin^2 \beta + 2e^c \sin \alpha \cos \alpha \sin \beta \cos \beta + e^{2c} \cos^2 \beta \sin^2 \alpha)}{2e^c \sin \alpha \sin \beta} \\ &= \frac{(e^{2c} + 1) \sin^2 \alpha \sin^2 \beta - 2e^c \sin \alpha \cos \alpha \sin \beta \cos \beta}{2e^c \sin \alpha \sin \beta} \\ &= \cosh c \sin \alpha \sin \beta - \cos \alpha \cos \beta. \end{aligned}$$

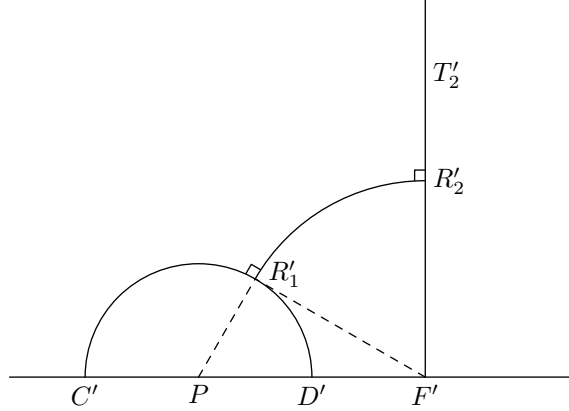


FIGURE 7.

□

4. POLYGON MODULES OF HYPERBOLIC SURFACES AND CANDIDATES OF SYSTOLES

By Corollary 2, to prove Theorem 1, we need only to work on a concrete module of hyperbolic surface Σ_g of given symmetry.

4.1. Polygon modules. (1) $4g$ -cyclic symmetry case: The hyperbolic surface of genus g with $4g$ -cyclic symmetry can be obtained by identifying opposite edges the regular hyperbolic $4g$ -polygon of angle sum 2π . Below we denote this surface by Σ_g^1 and the polygon by $P_{1,g}$, and often P_1 for short. Note all vertices in P_1 are identified to one point in Σ_g^1 . Each angle of $P_{1,g}$ is $2\pi/(4g)$. We often view P_1 as a polygon contained either in Σ_g^1 or in hyperbolic plane \mathbb{H}^2 .

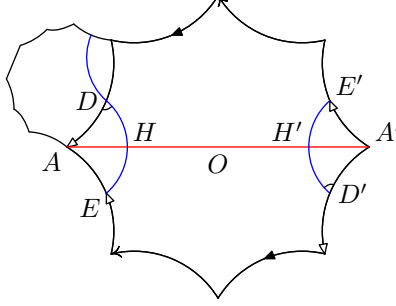


FIGURE 8.

For case of $4g + 2$ -cyclic symmetry we will pick two module.

(2) First polygon module of $4g + 2$ -cyclic case:

The hyperbolic surface of genus g with $4g + 2$ -cyclic symmetry can be obtained by identifying opposite edges the regular hyperbolic $4g+2$ -polygon of angle sum 4π . Below we denote this surface by Σ_g^2 and the polygon by $P_{2,g}$, often P_2 for short. Note all vertices in P_2 are alternatively identified to two points in Σ_g^2 . Each angle of P_2 is $2\pi/(2g + 1)$. We often view P_2 as a polygon contained either in Σ_g^2 or in the hyperbolic plane \mathbb{H}^2 .

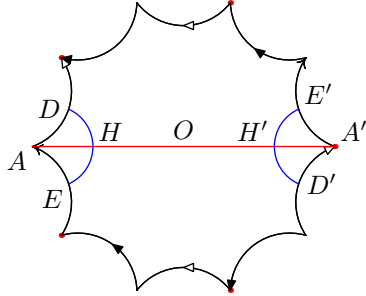


FIGURE 9.

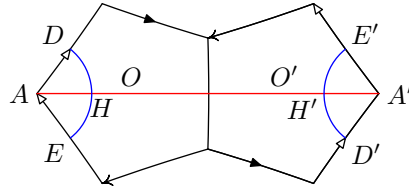


FIGURE 10.

(3) Dual fundamental region, the second polygon module of $4g + 2$ case.

For regular hyperbolic n -gon $P_i \subset \mathbb{H}^2$, $i = 1, 2$, defined above, $D_i(P_i)$ give a tessellation of \mathbb{H}^2 , where D_i is the deck transformation group such that $\mathbb{H}^2/D_i = \Sigma_g^i$. If two polygons in $D_i(P_i)$ share one edge, connect their centers by the unique geodesic arc. The union of those arcs form a lattice, which provide a new tessellation $D_i(P_i^*)$, where P_i^* is also a fundamental region of Σ_g^i .

One can check directly that

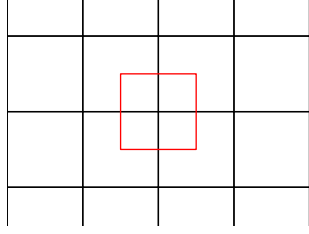


FIGURE 11.

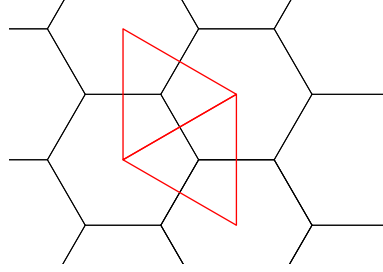


FIGURE 12.

Proposition 2. (1) P_1^* is congruent to P_1 , that is P_1^* is also a regular hyperbolic $4g$ -polygon of angle sum 2π . For each vertex A of P_1 , there is a unique P_1^* centered at A .

(2) While P_2^* is a union of two regular hyperbolic $2g+1$ polygons gluing along a pair of edges (see Figure 10), and each angle of the regular hyperbolic $2g+1$ polygon is $\pi/(2g+1)$. For each vertex A of P_2 , there is a unique P_2^* such that one of its regular $(2g+1)$ -gon centered at A .

Remark 1. (1) Figure 11 and Figure 12 are the genus one counterparts of $P_1(P_1^*)$ and $P_2(P_2^*)$ respectively.

(2) Σ_g^2 is also obtained by identifying opposite edges the hyperbolic $4g$ -polygon P_2^* . Note all vertices in P_2^* are identified to one point in Σ_g^2 . To see the $4g+2$ -cyclic symmetry on P_2^* directly, see [Wan91].

4.2. Candidates of systoles. In the regular polygons P_i , $i = 1, 2$, we call the geodesic that connects two opposite vertices a *diameter*. In P_2^* , call the geodesic connects two opposite vertices which is perpendicular to the common edge of two $2g+1$ -regular polygons a diameter.

Now we will use one polygon P below to present P_1 , P_2 and P_2^* . where O is the center of the whole P when P is either P_1 or P_2 , and is the center of one of two $2g+1$ polygon when $P = P_2^*$, AA' is a chosen diameter of the polygon P . Let D, E, D', E' be the mid-points of the corresponding edges neighboring the diameter. Then by symmetry it is not difficult to observe that the geodesic segments DE and $E'D'$ form a closed geodesic γ_i in Σ_g^i .

We are going to calculate the length of γ_i , $i = 1, 2$. Let a be the angle between OE and OA , and b be the half of the angle at the vertex of the polygon. Then (see Figure 13).

$$(4.1) \quad a = b = \frac{\pi}{4g} \text{ for } P_1; \quad 2a = b = \frac{2\pi}{4g+2} \text{ for } P_2; \quad a = 2b = \frac{2\pi}{4g+2}, \text{ for } P_2^*.$$

Proposition 3. In the polygons (see figure 13),

- (1) $\cosh |OD| = \cos b / \sin a$,
- (2) $\cosh |AD| = \cos a / \sin b$,
- (3) $\cosh |OA| = \cot a \cot b$,
- (4) $\sinh |DH| = \sqrt{\cos^2 a - \sin^2 b}$,
- (5) $\cosh |DE| = 2(\cos^2 a - \sin^2 b) + 1$,
- (6) $\cosh |AH| = \frac{\cos a}{\sin b \sqrt{\cos^2 a + \cos^2 b}}$,

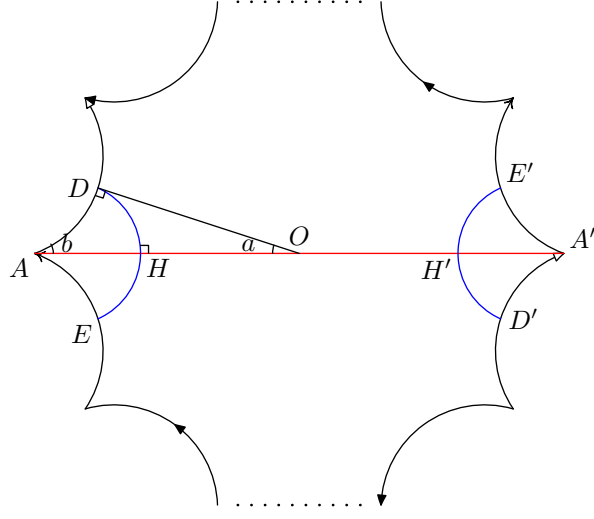


FIGURE 13.

$$(7) \sinh |AH| = \cot b \sqrt{\frac{\cos^2 a - \sin^2 b}{\cos^2 a + \cos^2 b}}.$$

In the surfaces the length of the geodesic γ_i ($DEE'D'$) is $2 \operatorname{arccosh}(1 + \cos 2a + \cos 2b)$.

Proof. In Figure 13, in the right-angle triangle $\triangle OAD$, $\angle ODA = \pi/2$, $\angle AOD = a$ and $\angle ODA = b$. Then by (3.4),

$$\cosh |OD| = \frac{\cos \angle OAD}{\sin \angle AOD} = \frac{\cos b}{\sin a},$$

and

$$\cosh |AD| = \frac{\cos \angle AOD}{\sin \angle DAO} = \frac{\cos a}{\sin b}.$$

By (3.2),

$$\cosh |OA| = \cosh |OD| \cosh |AD| = \cot a \cot b.$$

In the right-angled triangle $\triangle ADH$, $\angle DHA = \pi/2$, $\angle DAH = b$ and $\cosh |AD| = \cos a / \sin b$. Then by (3.3),

$$\begin{aligned} \sinh |DH| &= \sinh |AD| \sin \angle DAH \\ &= \sqrt{\left(\frac{\cos a}{\sin b}\right)^2 - 1} \sin b \\ &= \sqrt{\cos^2 a - \sin^2 b}. \end{aligned}$$

Therefore,

$$\begin{aligned} \cosh |DE| &= 2 \sinh^2 |DH| + 1 \\ &= 2 (\cos^2 a - \sin^2 b) + 1 \\ &= \cos 2a + \cos 2b + 1. \end{aligned}$$

Then $\cosh |DH| = \sqrt{\sinh^2 |DH| + 1} = \sqrt{\cos^2 a + \cos^2 b}$ and by (3.2),

$$\begin{aligned} \cosh |AH| &= \cosh |AD| / \cosh |DH| \\ &= \frac{\cos a}{\sin b \sqrt{\cos^2 a + \cos^2 b}}. \end{aligned}$$

$$\begin{aligned} \sinh |AH| &= \sqrt{\cosh^2 |DH| - 1} \\ &= \cot b \sqrt{\frac{\cos^2 a - \sin^2 b}{\cos^2 a + \cos^2 b}}. \end{aligned}$$

The length of the geodesic γ_i ($DEE'D'$) is equal to $2|DE|$. Thus by (5) we have

$$(4.2) \quad |\gamma_i| = 2 \operatorname{arccosh}(1 + \cos 2a + \cos 2b).$$

□

Let $2h_i$ be the length of γ_i , by plugging (4.1) into (4.2) we get

Corollary 3.

$$h_1 = \operatorname{arccosh}(\cos \pi/2g + 1) \text{ and } h_2 = \operatorname{arccosh}(1 + \cos \frac{\pi}{2g+1} + \cos \frac{2\pi}{2g+1})$$

5. INJECTIVE RADIOUS h_i

5.1. Some reductions. Now we begin to prove $2h_i$ is the systole of the hyperbolic surface Σ_g^i , $i = 1, 2$. By definitions and Proposition 3, we have the following

Claim 1. $B(x, h_i) \rightarrow \Sigma_g^i$ is an embedding for each $x \in \Sigma_g^i$ implies that $\operatorname{sys}(\Sigma_g^i) = 2h_i$, $i = 1, 2$.

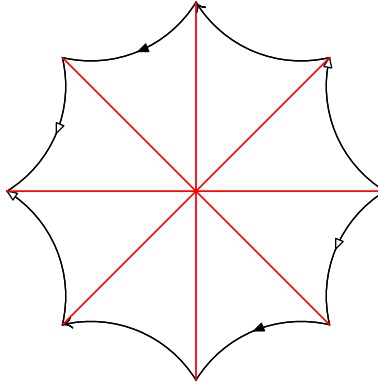


FIGURE 14.

We view P_i as a polygon contained in Σ_g^i . There is an observation that every closed essential geodesic in Σ_g^i must meet a diameter of P_i , since the diameters of P_i cut Σ_g^i into contractible pieces (see Figure 14). In particular each closed shortest geodesic meets a diameter of P_i . Note that all points in closed shortest geodesics have the same injective radius (see page [PAR06, p.178]).

Therefore we can reduce Claim 1 to the following:

Claim 2. $B(x, h_i) \rightarrow \Sigma_g^i$ is an embedding for each $x \in AA'$ implies that $\text{sys}(\Sigma_g^i) = 2h_i$, $i = 1, 2$.

Let H, H' be the intersections of the diameter AA' and the geodesic segment DE and $E'D'$ respectively, see Figure 13.

In each of the following two pictures Figure 15 and 16, the black polygon is P_i , and the green one is the dual polygon P_i^* around the vertex A , where Figure 15 is for $i = 1$ and Figure 16 is for $i = 2$. By symmetry and Claim 2, we need only consider $x \in OA \subset P_i$. Note $OA = OH \cup HA$ and A is the center of P_1^* in Figure 15 and the center of one of the two $2g + 1$ polygon of P_2^* . Moreover P_1^* is a polygon congruent to P_1 . We reduce Claim 2 to the following

Claim 3. (1) $B(x, h_1) \rightarrow \Sigma_g^1$ is an embedding for each $x \in OH \subset P_1$ implies that $\text{sys}(\Sigma_g^1) = 2h_1$;

(2) $B(x, h_2) \rightarrow \Sigma_g^2$ is an embedding for each $x \in OH \subset P_2$ and for each $x \in OH \subset P_2^*$ implies that $\text{sys}(\Sigma_g^i) = 2h_i$

We remind the reader that in P_2^* , O is the center of one of two $2g + 1$ polygons as is defined in Section 4.2.

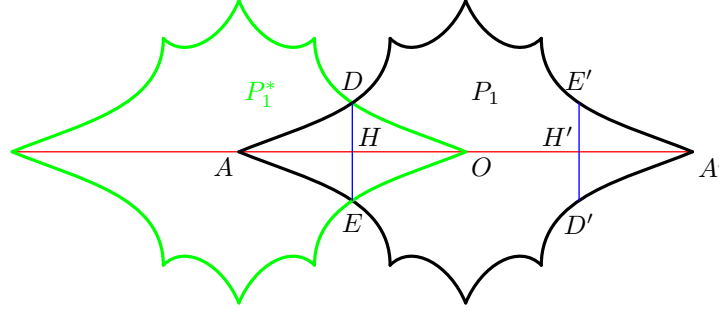


FIGURE 15.

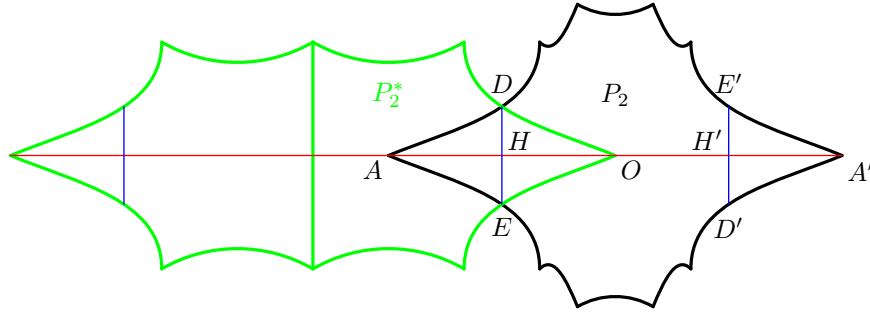


FIGURE 16.

5.2. Lift $B(x, h_i)$ to the universal cover. Below for $B(x, h_i)$ we assume that $x \in OH \subset P$.

Proposition 4. *For the polygon P ,*

(1) *The distance between any vertex in the polygons and the segment OH is bigger than h_i for $P = P_1, P_2, P_2^*$.*

(2) *The distance between an edge and the diameter AA' is larger than h_i except the nearest and second nearest edges for either $P = P_1$ and $g \geq 3$, or $P = P_2$ and $g \geq 2$, or $P = P_1^*$ and $g \geq 4$.*

Proof. (1) In Figure 17, AA' is a diameter of the polygon, O is the center of either $4g$ -gon P_1 , or $(4g+2)$ -gon P_2 , or the center of the $2g+1$ -gon of P_2^* containing A . V is a vertex of the polygon P_1, P_2 or the $2g+1$ polygon of P_2^* containing A .

. Thus $|OV| = |OA|$. By Proposition 3 (3), $\cosh |OV| = \cot a \cot b$. $\alpha = 2ka$, $k \in \mathbb{N}$. Distance between AA' and V is realized by $|VR|$. By (3.3),

$$\begin{aligned} \sinh |VR| &= \sinh |OV| \sin \alpha \\ &= \sqrt{\cot^2 a \cot^2 b - 1} \sin 2ka \\ &\geq \sqrt{\cot^2 a \cot^2 b - 1} \sin 2a. \end{aligned}$$

We use computer to compare $|VR|$ and h_i , finding that $|VR| \geq h_i$ if $P = P_1, P_2$ or the $2g+1$ polygon of P_2^* containing A . Vertices of the other $2g+1$ polygon of P_2^* do not meet $B(x, h_2)$ is a corollary of Proposition 4 (2).

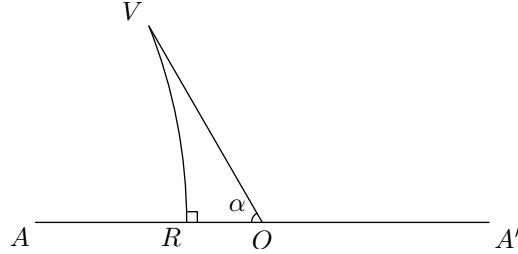


FIGURE 17.

(2) In Figure 18, AA' is a diameter and O is the center of P_1, P_2 or the center of the $2g+1$ polygon of P_2^* containing A . E is the mid-point of an edge of the polygon P_1, P_2 or the $2g+1$ polygon of P_2^* containing A . $|OE|$ is the distance from the edge to O . By Proposition 3 (1), $\cosh |OE| = \cos b / \sin a$. $\beta = (2k+1)a$, $k \in \mathbb{N}$. Distance between AA' and the edge is realized by $|R_1R_2|$. By (3.7),

$$\begin{aligned} \cosh |R_1R_2| &= \cosh |OE| \sin \beta \\ &= \frac{\cos b \sin(2k+1)a}{\sin a}. \end{aligned}$$

Then we compare $|R_1R_2|$ and h_i by computer. We get: $|R_1R_2| < h_i$ when $k \leq 2$; $|R_1R_2| \geq h_i$ when $k \geq 3$, if $P = P_1$ and $g \geq 3$ or $P = P_2$ and $g \geq 2$ or $P = P_2^*$ and $g \geq 4$. □

Proposition 5. *The upper half of a lift of $B(x, h_i)$ in \mathbb{H}^2 doesn't intersect any edges of the tessellation induced by the polygon other than edges AB_1, AB_2, B_1C_1 in Figure 19, if $P = P_1$ and $g \geq 4$; if $P = P_2$ and $g \geq 7$ or if $P = P_2^*$ and $g \geq 3$.*

This proposition characterizes the shape of $B(x, h_i)$.

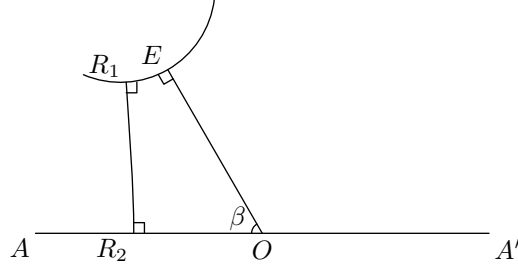


FIGURE 18.

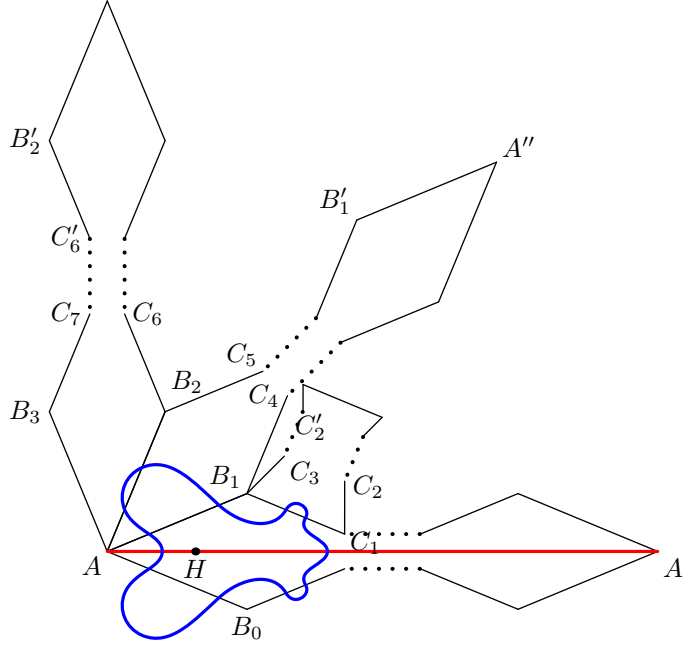


FIGURE 19.

Proof. By Proposition 4, $B(x, h_i)$ may intersect AB_1 and B_1C_1 in their interior in all of the three models.

First, we calculate the distance between the segment OH and AB_j ($j = 1, 2, 3$).

Lemma 1. *The distance between OH and AB_j ($j = 1, 2$) is smaller than h_i , while the distance between OH and AB_3 is bigger than h_i , if $P = P_1$ and $g \geq 4$, if $P = P_2$ and $g \geq 7$, if $P = P_2^*$ and $g \geq 3$.*

Proof. We calculate this result by Figure 21. In this figure, AA' is a diameter and AB_j is an edge. x is a point on AA' between H and O . Thus $\inf d(x, A) = |AH|$ for x between H and O . $\angle A = (2j - 1)b$. Then the infimum distance Rx between

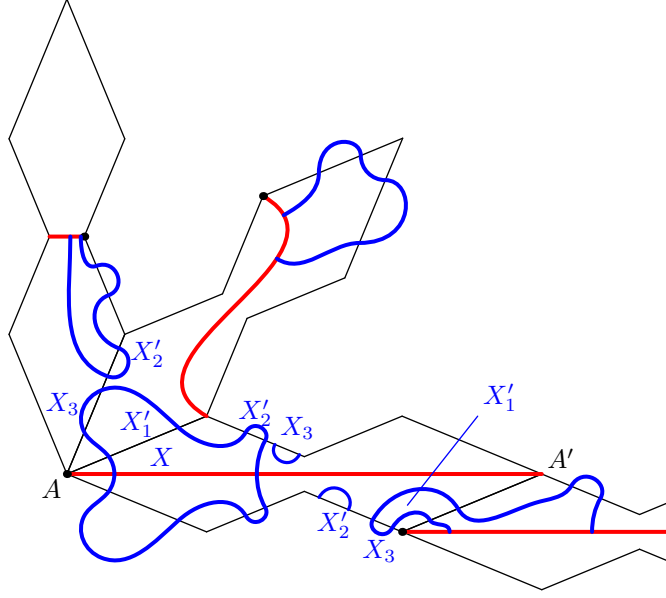


FIGURE 20.

x and AB_i is

$$\begin{aligned}
 \inf_{x \in OH} \sinh |Rx| &= \sin A \inf_{x \in OH} \sinh Ax \quad (\text{by (3.3)}) \\
 &= (\sin(2j-1)b) \sinh |AH| \\
 &= (\sin(2j-1)b) \cot b \sqrt{\frac{\cos^2 a - \sin^2 b}{\cos^2 a + \cos^2 b}} \quad (\text{by Prop. 3(2)})
 \end{aligned}$$

by (3.3). Then we compare $\inf_{x \in OH} |Rx|$ and h_i by computer programming. We get $\inf_{x \in OH} |Rx| \leq h_i$ for $j = 1, 2$ and $\inf_{x \in OH} |Rx| > h_i$ for $j = 3$, if $P = P_1$ and $g \geq 4$; if $P = P_2$ and $g \geq 7$ or if $P = P_2^*$ and $g \geq 3$. Therefore, the lemma is proved. \square

Lemma 1 is equivalent to say that $B(x, h_i)$ may intersect AB_1 or AB_2 , but won't meet AB_3 or any other further edges whose one vertex is A .

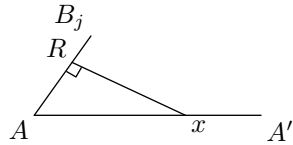


FIGURE 21.

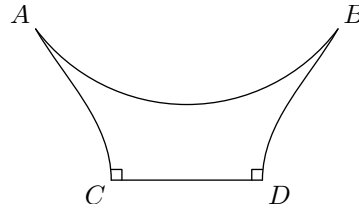


FIGURE 22.

Lemma 2. h_i is smaller than the distance between any two edges of the polygon that does not intersect.

Proof. It is sufficient to calculate the distance between two nearest non-intersecting edges in a polygon. In Figure 22, A, B are vertices of the polygon, $\angle A = \angle B = 2b$. AC and BD are parts of edges of the polygon. AB is an edge and thus $|AB| = 2 \operatorname{arccosh} \cos a / \sin b$ by Proposition 3. We calculate $|CD|$ by (3.11). Here

$$\begin{aligned} \cosh |CD| &= \cosh |AB| \cdot \sin \angle A \sin \angle B - \cos \angle A \cos \angle B \\ &= \left(\frac{2 \cos^2 a}{\sin^2 b} - 1 \right) \sin^2 2b - \cos^2 2b. \end{aligned}$$

We compare $|CD|$ with h_i , finding that $|CD| > h_i$ in all of the three models and obtain this conclusion. \square

By Lemma 2, the $B(x, h_i)$ doesn't meet any edges in Figure 19 except B_1C_3 , C_1C_2 , B_1C_4 , B_2C_6 and AB_j ($j = 1, 2$).

Lemma 3. $B(x, h_i)$ doesn't meet B_1C_4 and B_2C_6 .

Proof. The geodesic segment connecting the middle point of AB_0 and AB_1 is perpendicularly bisected by the diameter AA' ; the geodesic segment connecting the middle point of B_1A and B_1C_4 is perpendicularly bisected by the diameter $B_1B'_1$. The length of each segment is h_i by Proposition 3. These two geodesic segments form a new geodesic segment which is perpendicular to both AA' and $B_1B'_1$. Therefore, the distance between AA' and $B_1B'_1$ is h_i . Thus $B(x, h_i)$ doesn't meet B_1C_4 since segment B_1C_4 is farther to AA' than the line $B_1B'_1$.

Similarly, distance between the diameters $B_2B'_2$ and AA'' is not smaller than h_i . It implies that $B(x, h_i)$ doesn't meet B_2C_6 .

We remind the reader that the two endpoints of the common perpendicular between AA' and $B_1B'_1$ are H and H 's deck transformation image on $B_1B'_1$. This fact is useful in the proof of Corollary 1. \square

Lemma 4. $B(x, h_i)$ doesn't meet B_1C_3 and C_2C_1 .

Proof. First, we use Figure 23, which is a part of Figure 19, to calculate the distance between B_1C_3 and AA' in Figure 19. In Figure 23, AB_1 is an edge of the polygon and therefore its length is $2 \operatorname{arccosh} \cos a / \sin b$. $\angle A = b$ while $\angle B_1 = 4b$. Then the distance between AA' and B_1C_3 (realized by R_1R_2 in the figure) is

$$\begin{aligned} \cosh |R_1R_2| &= \sin \angle A \sin \angle B_1 \cosh |AB_1| - \cos \angle A \cos \angle B_1 \\ &= \sin b \sin 4b \left(2 \frac{\cos^2 a}{\sin^2 b} - 1 \right) - \cos b \cos 4b \end{aligned}$$

by (3.11). By computer calculation, we know this distance is larger than h_i in all of the three models.

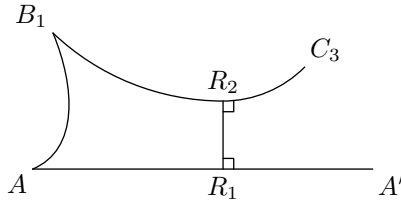


FIGURE 23.

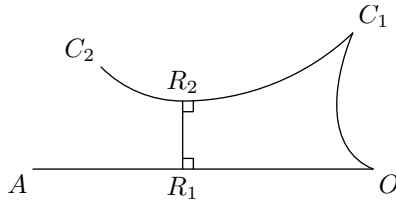


FIGURE 24.

Then, we use Figure 24, which is a part of Figure 19, to calculate the distance between C_1C_2 and AA' in Figure 19. In Figure 24, Since C_1 is a vertex of the regular polygon containing A , $|OC_1|$ is $\operatorname{arccosh} \cot a \cot b$. $\angle O = 4a$ while $\angle C_1 = 3b$. Then the distance, realized by R_1R_2 , between AA' and C_1C_2 is

$$\begin{aligned} \cosh |R_1R_2| &= \sin \angle O \sin \angle C_1 \cosh |OC_1| - \cos \angle A \cos \angle B_1 \\ &= \cot a \cot b \sin 4a \sin 3b - \cos 4a \cos 3b \end{aligned}$$

by (3.11). We compare this distance with h_i , finding that $|R_1R_2|$ is larger than h_i in all of the three models. \square

\square

Now we have proved Proposition 5, that is $B(x, h_i)$ in the universal cover \mathbb{H}^2 is shown as in Figure 19.

By projecting $B(x, h_i)$ from the universal cover to Σ_g^i , we will get a picture of $B(x, h_i) \subset P_i(P_i^*) \subset \Sigma_g^i$ shown as in Figure 25

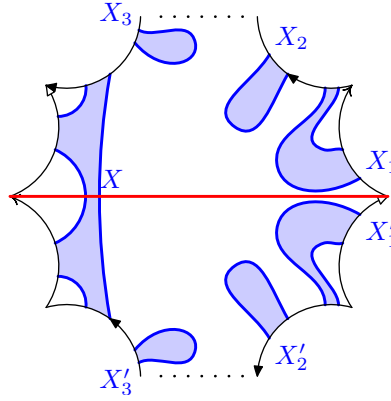


FIGURE 25.

5.3. Back to P . Now it is sufficient to prove that any two components in Figure 25 does not intersect.

Two components in the polygon do not intersect each other if and only if the corresponding disks (lifts of $B(x, h_i)$) in \mathbb{H}^2 does not intersect.

Lemma 5. *The interior of X_j does not meet the diameter AA' for $j = 1, 2, 3$*

Proof. X_1 's interior intersects AA' in Figure 25 if and only if in Figure 19, $B(x, h_i)$'s interior intersects the diameter $B_1B'_1$. But $d(AA', B_1B'_1) = h_i$. Thus X_1 's interior does not intersect AA' .

To prove X_2 in Figure 25 not meeting AA' , it is sufficient to prove in Figure 19, the distance between AA' and $C_2C'_2$ is larger than h_i .

In Figure 26, $d(AA', C_2C'_2)$ is realized by segment R_5R_6 . By using (3.7) in trirectangle with right angles R_5, R_1, R_2 and trirectangle with right angles R_6, R_3, R_4 , we have $|R_5R_6| > |R_3R_4| + |R_1R_2|$. We calculate $|R_3R_4|$ and $|R_1R_2|$ in the quadrilateral $R_3R_4B_1A$ and $R_1R_2C_1C_2$ respectively by (3.11). $\cosh |R_3R_4| = \cosh |AB_1| \sin \angle B_1AR_3 \sin \angle AB_1R_4 - \cos \angle B_1AR_3 \cos \angle AB_1R_4$ and $\cosh |R_1R_2| = \cosh |C_1C_2| \sin \angle R_1C_2C_1 \sin \angle C_2C_1R_2 -$

$\cos \angle R_1 C_2 C_1 \cos \angle C_2 C_1 R_2$. Here $\angle B_1 A R_3 = \angle R_1 C_2 C_1 = b$, $\angle A B_1 R_4 = \angle C_2 C_1 R_2 = 2b$, $|AB_1| = |C_1 C_2| = 2 \operatorname{arccosh} \cos b / \sin a$. Therefore,

$$\cosh |R_1 R_2| = \cosh |R_3 R_4| = \left(2 \frac{\cos^2 a}{\sin^2 b} - 1 \right) \sin 2b \sin b - \cos 2b \cos b.$$

We calculate $|R_1 R_2|$ and $|R_3 R_4|$ by computer, then compare $|R_1 R_2| + |R_3 R_4|$ with h_i and get the following conclusion: $|R_3 R_4| + |R_1 R_2| > h_i$, and $X_2 \cap AA' = \emptyset$ in Figure 25 for all of the three models.

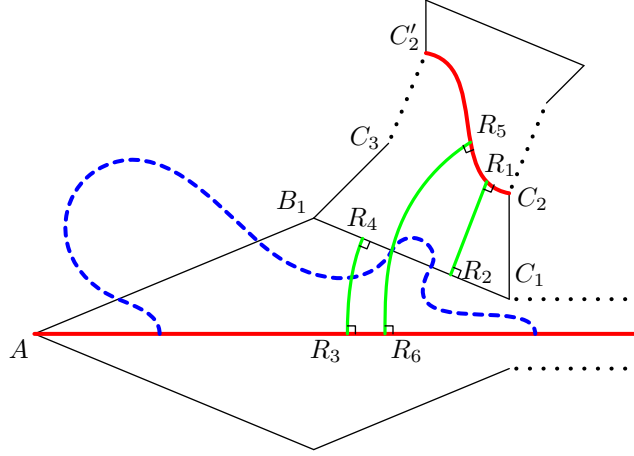


FIGURE 26.

X_3 in Figure 25 does not intersect AA' if and only if $B(x, h_i)$ in Figure 19 does not intersect the diameter $C_6 C_7$. $B(x, h_i)$ in Figure 19 does not intersect the diameter $C_6 C_7$, if $d(AA', C_6 C_7) > h_i$.

We use Figure 27 to calculate $d(AA', C_6 C_7)$. Figure 27 is a part of Figure 19. O' is the center of the regular polygon it is in. In the quadrilateral $AO'R_2 R_1$, $\angle A = 4b$, $\angle O' = 4a$, $|O'A| = \operatorname{arccosh} \cot a \cot b$ by Proposition 3. Then by (3.11),

$$\begin{aligned} \cosh |R_1 R_2| &= \cosh |AO'| \sin \angle A \sin \angle O' - \cos A \cos O' \\ (5.1) \quad &= \cot a \cot b \sin 4a \sin 4b - \cos 4a \cos 4b. \end{aligned}$$

By the help of the computer, we compare $|R_1 R_2|$ and h_i , finding that $|R_1 R_2|$ is larger than h_i for all of the three models. \square

Lemma 6. *In Figure 25, X_1, X_2, X_3 does not intersect X .*

Proof. (1) The distance between the polygon's center and an edge is $\cos b / \sin a$ by Proposition 3. Then we compare it with h_i by computer and the conclusion follows. For $g \geq 4$, distance between the polygon's center and edges are bigger than h_i . If X intersects X_1 or X_2 , there are two radii of $B(x, h_i)$ that intersect. It implies that the distance between two opposite edges is smaller or equal to $2h_i$, which is impossible. (See Figure 28.)

(2) $X \cap X_3 = \emptyset$ in Figure 25 is equivalent to in Figure 19, the distance between x on AA' and its deck transformation image on $C_6 C_7$ is larger than $2h_i$. (See

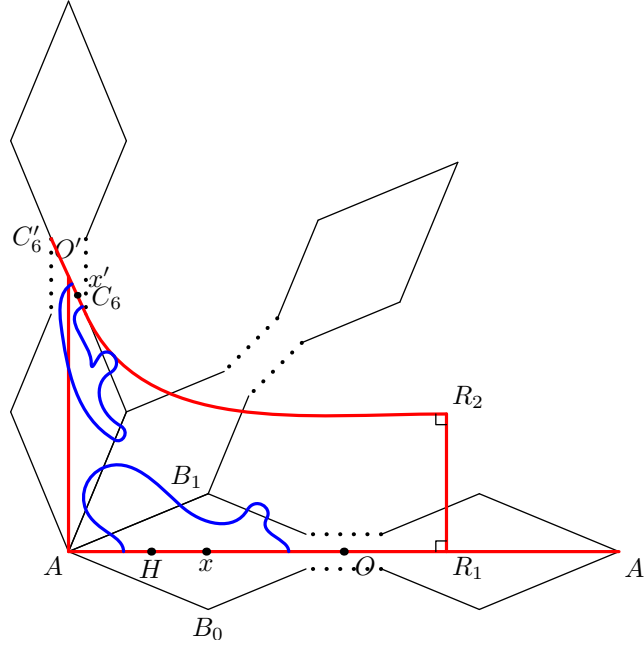


FIGURE 27.

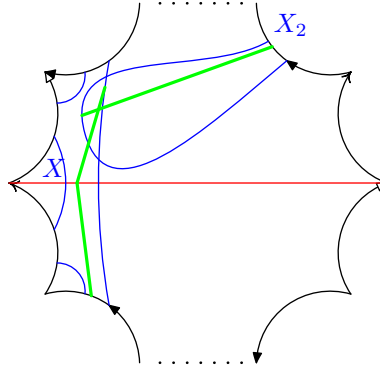


FIGURE 28.

Figure 27) Now we prove this distance is larger than $2h_i$ by the formulae of the quadrilateral:

x is a point moving on the diameter AA' between H and O . x' is its deck transformation image. x' moves as x moves. We calculate $\inf_{x \in HO} d(x, x')$ and compare it with $2h_i$.

In Figure 27, we have obtained $|R_1 R_2|$ in (5.1). Then in the quadrilateral $R_1 R_2 x' x$, by (3.10),

$$\cosh |xx'| = \cosh |R_1 R_2| \cosh |R_1 x| \cosh |R_2 x'| - \sinh |R_1 x| \sinh |R_2 x'|.$$

Assume $|Ax| = t$, then $|R_1x| = |AR_1| - t$ and $|R_2x'| = |R_2C_6| + t$. Here $|C_6x'| = |Ax| = t$. $|AH| \leq t \leq |AO|$. Here H is the intersecting point of the diameter and the geodesic connecting the mid-point of AB_0 and AB_1 .

Then we denote $\cosh |xx'|$ to be $f(t)$.

$$f(t) = \cosh |R_1R_2| \cosh(|AR_1| - t) \cosh(|C_6R_2| + t) - \sinh(|AR_1| - t) \sinh(|C_6R_2| + t).$$

Thus

$$\begin{aligned} f'(t) &= \cosh |R_1R_2| (-\sinh(|AR_1| - t) \cosh(|C_6R_2| + t) + \cosh(|AR_1| - t) \sinh(|C_6R_2| + t)) - \\ &\quad (-\cosh(|AR_1| - t) \sinh(|C_6R_2| + t) + \sinh(|AR_1| - t) \cosh(|C_6R_2| + t)) \\ &= (\cosh |R_1R_2| - 1) \sinh(2t - |AR_1| + |C_6R_2|). \end{aligned}$$

Therefore, the minimum of $f(t)$ is obtained when $t = (|AR_1| - |C_6R_2|)/2$. At this point, $|R_1x| = |R_2x'| = (|AR_1| + |C_6R_2|)/2$ and thus quadrilateral $xx'R_2R_1$ is a quadrilateral with $\angle R_1 = \angle R_2 = \pi/2$, $\angle x = \angle x'$. Moreover, $|Ax| + |O'x'| = |AO|$. ($|O'x'| = |O'C_6| - |C_6x'| = |AO| - |Ax|$.)

To prove $|xx'| > 2h_i$, we construct a quadrilateral $R_1R_2S_2S_1$. (See Figure 29) In the quadrilateral $R_1R_2O'A$, $\angle A = 4b$ and $\angle O' = 4a$. Without loss of generality, we assume $b \geq a$. $S_1 \in AR_1$, $S_2 \in O'R_2$, satisfying $\angle S_1S_2R_2 = \angle S_2S_1R_1 = 4b$. (We remark that when $a = b$, $S_1 = A$ and $S_2 = O'$). Such S_1 and S_2 exist on the segment R_1A and R_2O' respectively instead of on the extended lines of R_1A and R_2O' because otherwise we'll get a quadrilateral with sum of interior angles bigger than 2π or a triangle with sum of interior angles bigger than π , which is impossible.

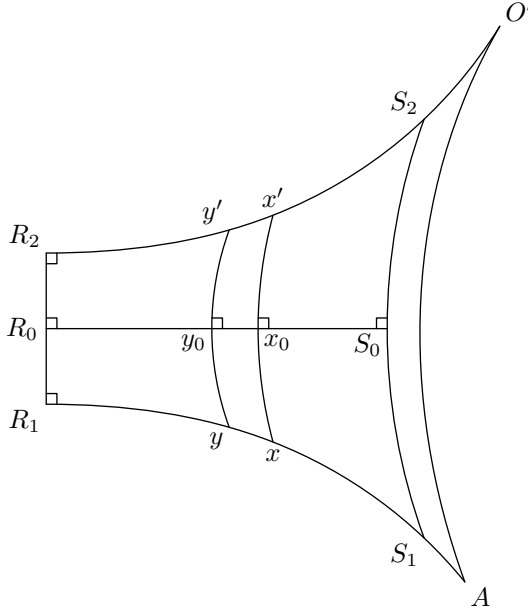


FIGURE 29.

Then we pick up two points y, y' on R_1S_1 and R_2S_2 respectively, satisfying $|S_1y| = |S_2y'| = |AO|/2$. Then $|R_1x| \geq |R_1y|$ and $|R_2x'| \geq |R_2y'|$ by the following argument: We have $|R_1A| \geq |R_1S_1|$, $|R_2O'| \geq |R_2S_2|$ and $|Ax| + |O'x'| = |AO|$. Without loss of generality, we assume $|Ax| \leq |AO|/2 \leq |O'x'|$. Then $|R_1y| =$

$|R_1S_1| - |S_1y| = |R_1S_1| - |AO|/2 \leq |R_1A| - |Ax| = |R_1x|$. Then $|R_2y'| \leq |R_2x'|$ follows from $|R_1x| = |R_2x'|$ and $|R_1y| = |R_2y'|$. This result means $|xx'| \geq |yy'|$ by (3.11).

To prove $|xx'| \geq 2h_i$, it is sufficient to prove $|yy'| \geq 2h_i$. Now we calculate $|yy'|$ and compare it with $2h_i$. By the symmetry of the quadrilaterals $R_1R_2y'y$, $R_1R_2x'x$ and $R_1R_2S_2S_1$, the segment R_0S_0 divides each of these quadrilaterals into two equal trirectangles, namely $R_0R_1yy_0$ and $R_0R_2y'y_0$; $R_0R_1xx_0$ and $R_0R_2x'x_0$; $R_0R_1S_1S_0$ and $R_0R_2S_2S_0$. Here R_0 , y_0 , x_0 and S_0 are the middle points of R_1R_2 , yy' , xx' and S_1S_2 respectively. Thus $|yy'| \geq 2h_i$ is equivalent to $|yy_0| \geq h_i$. Now we calculate $|yy_0|$.

By our construction, in the trirectangle $R_1R_0S_0S_1$, $\angle R_0 = \angle R_1 = \angle S_0 = \pi/2$, $\angle S_1 = 4b$. $|R_1R_2|$ is obtained in (5.1). Then we get $\coth \frac{|R_1R_2|}{2}$:

$$\begin{aligned} \cosh \frac{|R_1R_2|}{2} &= \sqrt{\frac{\cosh |R_1R_2| + 1}{2}} \\ &= \sqrt{\frac{\cot a \cot b \sin 4a \sin 4b - \cos 4a \cos 4b + 1}{2}}, \\ \sinh \frac{|R_1R_2|}{2} &= \sqrt{\frac{\cosh |R_1R_2| - 1}{2}} \\ &= \sqrt{\frac{\cot a \cot b \sin 4a \sin 4b - \cos 4a \cos 4b - 1}{2}}, \\ \coth \frac{|R_1R_2|}{2} &= \cosh \frac{|R_1R_2|}{2} / \sinh \frac{|R_1R_2|}{2} \\ &= \sqrt{\frac{\cot a \cot b \sin 4a \sin 4b - \cos 4a \cos 4b + 1}{\cot a \cot b \sin 4a \sin 4b - \cos 4a \cos 4b - 1}}. \end{aligned}$$

Then by (3.9), we obtain $|R_1S_1|$:

$$\begin{aligned} \sinh |R_1S_1| &= \coth \frac{|R_1R_2|}{2} \cot \angle S_0S_1R_1 \\ &= \coth \frac{|R_1R_2|}{2} \cot 4b \end{aligned}$$

Then we obtain $|R_1y|$:

$$\begin{aligned} \cosh |R_1y| &= \cosh(|R_1S_1| - |S_1y|) \\ &= \cosh(|R_1S_1| - |AO|/2) \\ &= \cosh |R_1S_1| \cosh \frac{|AO|}{2} - \sinh |R_1S_1| \sinh \frac{|AO|}{2} \end{aligned}$$

Here $|AO| = \operatorname{arccosh}(\cot a \cot b)$.

Finally, we get $|yy_0|$ by (3.8):

$$\sinh |yy_0| = \sinh |R_0R_1| \cosh |R_1y|$$

By computer programming, we compare yy_0 and h_i , finding that $yy_0 > h_i$ and therefore $X \cap X_3 = \emptyset$ in Figure 27.

We remark that the proof above also proves $X_1 \cap X_2 = \emptyset$, see Figure 27.

□

Lemma 7. *In Figure 25, X_1, X_2, X_3 do not intersect each other when $g \geq 4$.*

Proof. The proof of $X \cap X_3 = \emptyset$ in Lemma 6 also proves $X_1 \cap X_2 = \emptyset$. Below we prove (1) $X_2 \cap X_3 = \emptyset$ (2) $X_1 \cap X_3 = \emptyset$.

In P_1 model, we pick the diameter perpendicular to AA' (denoted BB'). Now we prove that X_1, X_2, X_3 cannot meet BB' , and therefore $X_1 \cap X_3 = \emptyset$ and $X_2 \cap X_3 = \emptyset$. (See Figure 30.)

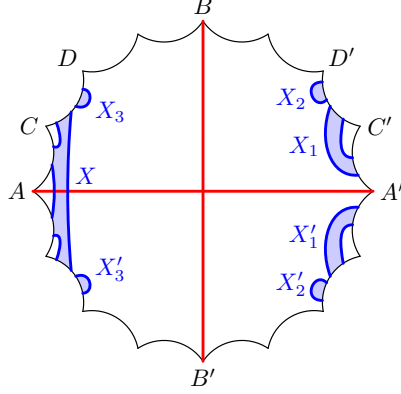


FIGURE 30.

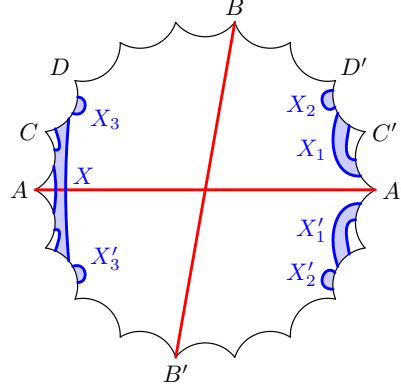


FIGURE 31.

The proof of $X_i \cap BB' = \emptyset$ are exactly the same for $i = 1, 2, 3$. Without loss of generality, we prove that $X_3 \cap BB' = \emptyset$. , In Figure 30, we denote the edge that meets X_3 to be CD . Since $g \geq 4$, the edge CD is not the nearest and the second nearest edge to the diameter BB' , by Proposition 4 (2), $d(BB', CD) > h_i$. On the other hand, the center x' of the $B(x', h_i)$ containing X_3 is outside the polygon in Figure 30. Therefore, $\forall x_3 \in X_3, d(x_3, CD) \leq h_i$. Thus $X_3 \cap BB' = \emptyset$.

In P_2 model, let BB' be one of the diameters whose angle with AA' is the biggest, see Figure 31. Since $g \geq 4$ and P_2 is $4g+2$ gon, we still can apply Proposition 4 (2) to prove $X_i \cap BB' = \emptyset$ for $i = 1, 2, 3$ exactly as P_1 case, and then $X_1 \cap X_3 = \emptyset$, $X_2 \cap X_3 = \emptyset$.

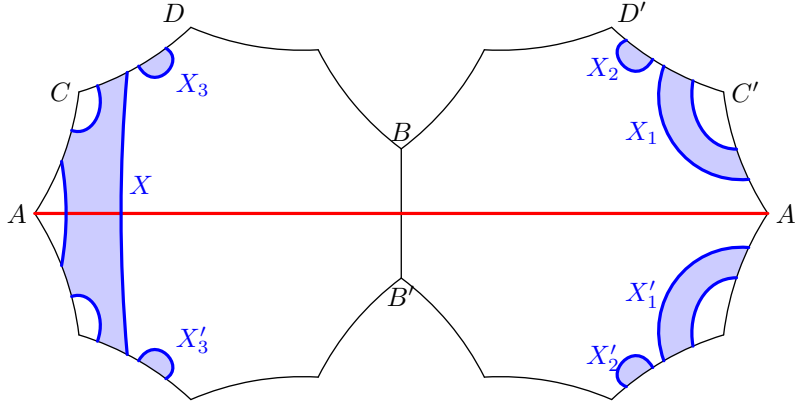


FIGURE 32.

In P_2^* model, we let BB' be the edge separate the two $2g + 1$ polygons and the edge that meets X_3 be CD (See Figure 32) Since $g \geq 4$, $2g + 1 \geq 9$, the edge CD and the edge BB' are disjoint. Then by Lemma 2, $d(BB', CD) > h_i$. On the other hand, the center x' of the $B(x', h_i)$ that corresponds to X_3 is outside the polygon in Figure 32. Therefore, $\forall x_3 \in X_3$, $d(x_3, CD) \leq h_i$. Thus $X_3 \cap BB' = \emptyset$.

By exactly the same proof, we have $X_i \cap BB' = \emptyset$ for $i = 1, 2$. So that $X_1 \cap X_3 = \emptyset$ and $X_2 \cap X_3 = \emptyset$.

We have proved the theorem. □

Now we begin to prove Corollary 1.

Corollary 1. *In Σ_g^1 , there are $2g$ closed geodesics having length $\text{sys}(\Sigma_g^1)$ and in Σ_g^2 , there are $2g + 1$ closed geodesics having length $\text{sys}(\Sigma_g^2)$.*

Proof. By the proof of Lemma 5, Lemma 6 and Lemma 7, each pair of components in Figure 25 does not intersect except X_1 and X'_1 . X_1 and X'_1 may be tangent to each other. For a fixed x (center of the ball $B(x, h_i)$) on OH , the number of points in $\partial X_1 \cap \partial X'_1$ is 0 or 1 by the convexity of balls in hyperbolic plane. The only thing to show is $\partial X_1 \cap \partial X'_1 \neq \emptyset$ if and only if x is the point H .

This fact is straight forward by the proof of Lemma 3. In that proof, the common perpendicular between AA' and $B_1B'_1$ in Figure 19 is the segment connecting H and H 's deck transformation image on $B_1B'_1$. Besides, $d(AA', B_1B'_1) = h_i$. Therefore $d(x, B_1B'_1) \geq h_i$, $\forall x \in OH$. The equality holds if and only if $x = H$. It proves that in Figure 25, $X_1 \cap AA' = \{H'\}$ and $X'_1 \cap AA' = \{H'\}$ if and only if $x = H$. (Here H' is the intersecting point of $E'D'$ and AA' in Figure 13.)

Then it proves that γ_i ($DEE'D'$ in Figure 13) is the unique systole that intersects OH in all of the three models. By Claim 3, γ_i is the unique systole that intersects OA in P_1 and P_2 . By the invariance of γ_i under the π -rotation of P_1 and P_2 , γ_i is the unique systole that intersects AA' in P_1 and P_2 . This is equivalent to that given a diameter of P_1 or P_2 , there is a unique systole intersects the diameter. Therefore by counting the number of diameters of P_1 and P_2 , the Corollary holds. □

6. APPENDIX

In this Section, we give the source code and figure for the comparison between $|CD|$ and h_i in Lemma 2. The code is written in MATLAB. The codes for other comparisons are similar.

```

1
2 %P_1 model
3 a = [eps:eps:pi/8];
4 b = a;
5 %P_2 model
6 %a = [eps:eps:pi/10];
7 %b = 2*a;
8 %P_2^* model
9 %a = [eps:eps:pi/5];
10 %b = 0.5*a;
11

```

```

12 chdst = (2*(cos(a)./sin(b)).^2-1).*(sin(2*b)).^2-(cos
    (2*b)).^2;
13
14 chh = 1 + cos(2*a) + cos(2*b);
15 %shh = sqrt(chh.^2-1);
16 f = chdst - chh;
17 plot(a,f);

```

Figure 33 shows the result of the comparison in P_1 model. In Figure 33, the horizontal axis is the variable a , while the vertical axis is $\cosh |CD| - \cosh h_i$ (depends on a).

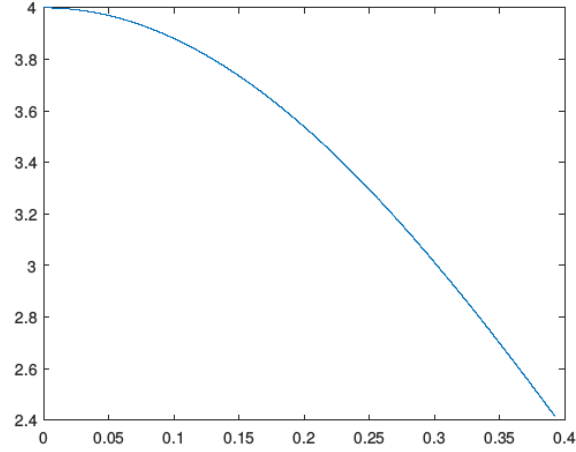


FIGURE 33.

REFERENCES

- [Bav92] Christophe Bavard. La systole des surfaces hyperelliptiques. *Prepubl. Ec. Norm. Sup. Lyon*, 71, 1992.
- [BS94] Peter Buser and Peter Sarnak. On the period matrix of a riemann surface of large genus (with an appendix by jh conway and nja sloane). *Inventiones mathematicae*, 117(1):27–56, 1994.
- [Bus10] Peter Buser. *Geometry and spectra of compact Riemann surfaces*. Springer Science & Business Media, 2010.
- [GWWZ15] Yu Guo, Chao Wang, Shicheng Wang, and Yimu Zhang. Embedding periodic maps on surfaces into those on s^3 . *Chinese Annals of Mathematics, Series B*, 36(2):161180, March 2015.
- [Hu] A. Hurwitz, *Über algebraische Gebilde mit eindeutigen Transformationen in sich*, Math. Ann. 41 (1893), 403-442
- [Jen84] Felix Jenni. Über den ersten eigenwert des laplace-operators auf ausgewählten beispielen kompakter riemannscher flächen. *Commentarii Mathematici Helvetici*, 59(1):193–203, 1984.
- [KSV07] Mikhail G Katz, Mary Schaps, Uzi Vishne, Logarithmic growth of systole of arithmetic riemann surfaces along congruence subgroups. *Journal of Differential Geometry*, 76(3):399–422, 2007.

- [Kul97] Ravi S Kulkarni. Riemann surfaces admitting large automorphism groups. *Extremal Riemann surfaces (San Francisco, CA, 1995)*, 201:63–79, 1997.
- [Par14] Hugo Parlier. Simple closed geodesics and the study of teichmüller spaces. *Handbook of Teichmüller Theory, Volume IV*, pages 113–134, 2014.
- [PAR06] Peter Petersen, S Axler, and KA Ribet. *Riemannian geometry*, volume 171. Springer, 2006.
- [Pet18] Bram Petri. Hyperbolic surfaces with long systoles that form a pants decomposition. *Proceedings of the American Mathematical Society*, 146(3):1069–1081, 2018.
- [PW15] Bram Petri and Alexander Walker. Graphs of large girth and surfaces of large systole. *arXiv preprint arXiv:1512.06839*, 2015.
- [Sch93] P Schmutz. Riemann surfaces with shortest geodesic of maximal length. *Geometric & Functional Analysis GAFA*, 3(6):564–631, 1993.
- [Wan91] Shicheng Wang. Maximum orders of periodic maps on closed surfaces. *Topology and its Applications*, 41(3):255–262, 1991.
- [Wim95] A. Wiman, *Über die hyperelliptischen Kurven und diejenigen vom Geschlecht $p=3$, welche eindeutige Transformationen in sich zulassen*, Bihang Till. Kongl. Svenska Vetenskaps-Akademiens Handlingar 21 (1) 1895.

SCHOOL OF MATHEMATICAL SCIENCES, PEKING UNIVERSITY, BEIJING 100871, CHINA
E-mail address: `barries@163.com`

SCHOOL OF MATHEMATICAL SCIENCES, PEKING UNIVERSITY, BEIJING 100871, CHINA
E-mail address: `yue_gao@pku.edu.cn`

SCHOOL OF MATHEMATICAL SCIENCES, PEKING UNIVERSITY, BEIJING 100871, CHINA
E-mail address: `wangsc@math.pku.edu.cn`